

Information engine in a nonequilibrium bath

Tushar K. Saha,^{1,*} Jannik Ehrich,^{1,2,*} Momčilo Gavrilov,¹ Susanne Still,² David A. Sivak,¹ and John Bechhoefer¹

¹*Department of Physics, Simon Fraser University, Burnaby, BC, V5A 1S6 Canada*

²*Department of Physics and Astronomy, University of Hawaii at Mānoa, Honolulu, HI 96822, USA*

(Dated: August 2, 2022)

Information engines can convert thermal fluctuations of a bath at temperature T into work at rates of order $k_B T$ per relaxation time of the system. We show experimentally that such engines, when in contact with a bath that is out of equilibrium, can extract much more work. We place a heavy, micron-scale bead in a harmonic potential that ratchets up to capture favorable fluctuations. Adding a fluctuating electric field increases work extraction up to ten times, limited only by the strength of applied field. Our results connect Maxwell’s demon with energy harvesting and an estimate of efficiency shows that information engines in nonequilibrium baths can greatly outperform conventional engines.

Maxwell’s famous thought experiment proposed a way to convert information about thermal fluctuations into energy [1]. Exploring “Maxwell demons” has improved our understanding of the second law of thermodynamics [2, 3]. Building them, as “information engines”, a concept inspired originally by Szilard’s model [4], has allowed tests of the second law applied to mesoscopic length scales [5–10]. The ability of an information engine to extract work from a single heat bath is reconciled with the second law because the cost of sensing fluctuations and exploiting the relevant information equals or exceeds the energy extracted [3, 4, 11, 12].

That information-processing costs compensate for the extracted energy implicitly assumes that the measuring device operates at the same temperature as the engine itself. If the temperature of the engine bath exceeds that of the bath connected to the measuring device, net work can be extracted [13]. But the range of temperatures available for heat baths is small, which limits engine power, even with optimized information processing [14]. For example, the ratio of boiling-water to freezing-water temperatures is $373/273 \approx 1.4$, and the ratio of temperatures in an internal-combustion heat engine is $\lesssim 8$, with practical efficiencies $\lesssim 0.5$ [15].

In this paper, we show experimentally that this limitation can be overcome by immersing the information engine in a nonequilibrium heat bath. The environment is out of equilibrium at macroscopic scales but has practically unchanged local temperature T . The measuring device of the engine is in contact with an equilibrium heat bath also at temperature T . Such an information engine extracts energy from both thermal and nonequilibrium fluctuations. Similar ideas have been proposed theoretically to take advantage of active fluctuations produced by bacteria swimming in a bath [16] and to increase the output of a Szilard engine [17].

With carefully chosen experimental parameters, our engine can extract work at up to ten times the maximum rate achievable when connected to an equilibrium bath at temperature T . Moreover, we show that energy extraction is constrained only by practical experimental

limits on the nonequilibrium forcing of the external environment. The energy extracted can, in principle, exceed the costs associated with necessary information processing and control by orders of magnitude.

Experimental setup.—The information engine consists of an optically trapped, heavy bead in water that acts as a thermal bath at room temperature T [18]. To force the bath out of equilibrium, a fluctuating electric field is applied via electrodes [19], as shown in Fig. 1(a). Unlike previous experimental implementations of baths with higher effective temperatures that were based on digitally generated noise [19–22], the fluctuating field here arises from a physical reservoir, the amplified Johnson voltage noise of a resistor at temperature T . The nonequilibrium-noise strength is regulated by a variable-gain amplifier, whose bandwidth is set by a low-pass filter with adjustable cutoff frequency. Under gravity, the bead fluctuates about a mean position because of thermal and nonequilibrium forces acting on it. Further details on the setup are given in the Appendix.

System dynamics.—We model the trapped bead as a spring-mass system, as shown in Fig. 1(b). The information engine operates by raising the trap position when the bead fluctuates above the trap center. The upward fluctuation of the bead, increasing its gravitational potential energy, is rectified by ratcheting the trap position. We update the trap position to convert the thermal fluctuations from the nonequilibrium bath into gravitational energy, carefully choosing the distance the trap is moved, so that the shifted trap potential does not perform work on the bead [18].

The position $x(t)$ of a bead trapped in a harmonic potential centered on λ at time t in a nonequilibrium bath is described by the Langevin equation

$$\dot{x}(t) = - \underbrace{[x(t) - \lambda(t)]}_{\text{restoring force}} - \underbrace{\delta_g}_{\text{grav.}} + \underbrace{\xi(t)}_{\text{thermal}} + \underbrace{\zeta(t)}_{\text{noneq.}}, \quad (1)$$

where we have rescaled lengths by the bead position’s equilibrium standard deviation $\sigma \equiv k_B T / \kappa$ in the trap with strength κ , and times by the relaxation time $\tau_r \equiv$

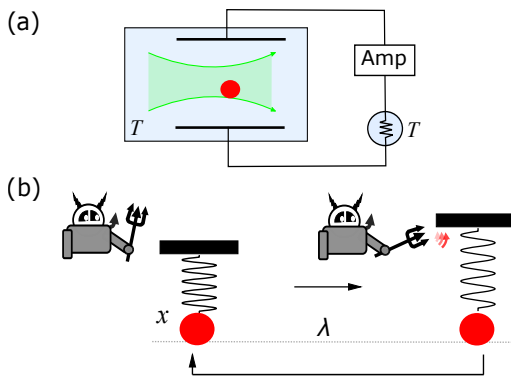


FIG. 1. Schematic of information engine in a nonequilibrium bath. (a) Optically trapped bead in water, subject to non-equilibrium external noise. This external noise is generated by electrodes connected to a resistor in a thermal bath, followed by an amplifier. Both bead and resistor are at room temperature T . (b) Schematic of the information engine.

γ/κ of a bead with Stokes' friction coefficient γ in the trap. The scaled effective mass $\delta_g \equiv \Delta mg/(\kappa\sigma)$ accounts for the effects of gravity and buoyancy on a bead with effective mass $\Delta m = \Delta\rho(4/3)\pi r^3$, with r the particle radius and $\Delta\rho$ the density difference between particle and the surrounding fluid. The noise $\xi(t)$ reflects equilibrium thermal fluctuations of the water bath and is modeled by Gaussian white noise with zero mean and variance $\langle \xi(t)\xi(t') \rangle = 2\delta(t-t')$.

We measure the bead position at a sampling time $t_s = 20 \mu\text{s}$, using the forward-scattered light from a detection laser. The trap is updated at the same time that measurements are made, responding to measurements that took place $20 \mu\text{s}$ in the past. The ratchet feedback algorithm is

$$\lambda_{k+1} = \lambda_k + \alpha (x_k - \lambda_k) \Theta(x_k - \lambda_k), \quad (2)$$

for Heaviside (step) function $\Theta(\cdot)$ and scalar feedback gain α .

Nonequilibrium bath.—The second noise $\zeta(t)$ in Eq. (1) describes random electrokinetic forcing of strength D_{ne} . The electrokinetic forces combine electroosmotic and electrophoretic effects on the bead [23]. Here, we empirically determine the nonequilibrium-noise strength.

The fluctuating electrokinetic forces arise from the amplified, low-pass-filtered Johnson noise of a resistor. In scaled units, the noise term obeys

$$f_{\text{ne}}^{-1} \dot{\zeta}(t) = -\zeta(t) + \sqrt{D_{\text{ne}}} \tilde{\xi}(t), \quad (3)$$

where f_{ne} is the *cutoff* frequency set by the filter frequency, $\langle \tilde{\xi}(t) \rangle = 0$, and $\langle \tilde{\xi}(t)\tilde{\xi}(t') \rangle = 2\delta(t-t')$. The low-pass filter generates exponentially correlated colored nonequilibrium Ornstein-Uhlenbeck noise, $\langle \zeta(t)\zeta(t') \rangle = D_{\text{ne}} f_{\text{ne}} e^{-f_{\text{ne}}|t-t'|}$, which tends to white noise for $f_{\text{ne}} \rightarrow$

∞ . The dynamics of particles subjected to such noise have been studied extensively [24–27]. In experiments, we can vary D_{ne} from 0 to 83.5 and f_{ne} from 10 Hz to 24 kHz. The trap's cutoff frequency $f_c = 1/(2\pi\tau_T)$ is 200 ± 2 Hz.

Energy measurements.— At each time step, the stored gravitational (free) energy of the bead changes by

$$\Delta F_{k+1} = \delta_g (\lambda_{k+1} - \lambda_k). \quad (4)$$

The average output power is measured using $\dot{F} = \sum_{k=0}^N \langle \Delta F_k \rangle / Nt_s$, where the ensemble average $\langle \cdot \rangle$ is estimated by averaging over multiple trajectories, each of length N time steps.

The work done by the trap on the bead is

$$W_{k+1} = \frac{1}{2} [(x_{k+1} - \lambda_{k+1})^2 - (x_{k+1} - \lambda_k)^2], \quad (5)$$

and the average trap power is measured using $\dot{W} = \sum_{k=0}^N \langle W_k \rangle / Nt_s$.

Equation (5) implies that the trap power would be zero for $\alpha = 2$ if there were no feedback delay and no measurement uncertainty [18]; however, the one-step delay implies that the zero-work condition is realized at a lower feedback gain, empirically $\alpha \approx 1.8$, when measurement noise is negligible [28].

Results.—We study the dependence of the information engine's output power on the characteristics of the non-equilibrium noise.

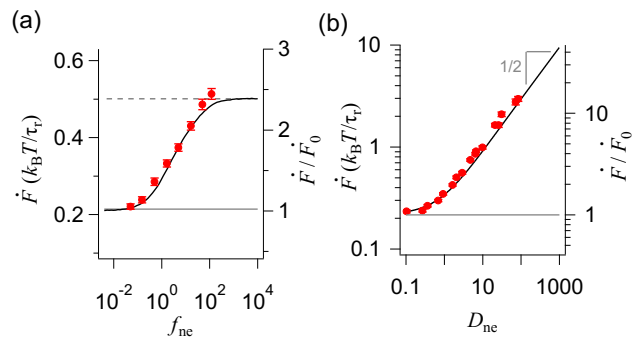


FIG. 2. Output-power optimization for a 3- μm bead at $\alpha = 1.8$. (a) Output power as a function of cutoff frequency f_{ne} of the nonequilibrium bath scaled by the trap cutoff frequency f_c , at nonequilibrium-noise strength $D_{\text{ne}} = 3.0$ and scaled mass $\delta_g = 0.37$. Dashed line: high- f_{ne} limit, from Eq. (9). Gray line: measured output power \dot{F}_0 at equilibrium ($D_{\text{ne}} = 0$). Black curve: prediction based on numerical simulations, using the measured D_{ne} ; not a fit. Right axis: ratio of nonequilibrium to equilibrium output powers. (b) Output power as a function of D_{ne} for high cutoff frequency ($f_{\text{ne}} = 118$). Gray line: measured output power at $D_{\text{ne}} = 0$ and $\delta_g = 0.38$. Black curve: scaling-theory prediction from Eq. (9), showing the asymptotic $\sim D_{\text{ne}}^{1/2}$ dependence.

First, we measure the output power \dot{F} for different noise cutoff frequencies f_{ne} , at fixed amplitude $D_{\text{ne}} = 3.0$.

Figure S4(a) shows that the output power increases with f_{ne} , in agreement with numerical simulations (see Appendix). The output power saturates at $f_{\text{ne}} \gtrsim 100$: At high f_{ne} , the bead cannot follow the force fluctuations and thus effectively experiences white noise indistinguishable from that of a thermal bath with a higher “effective temperature.” Further increases in the cutoff frequency do not affect the bead’s dynamics. At low f_{ne} , the nonequilibrium fluctuations are weaker than the equilibrium thermal fluctuations, and the output power equals that in a thermal bath at room temperature. At the maximum f_{ne} , the output power for $D_{\text{ne}} = 3.0$ is more than twice ($2.4\times$) that for a purely thermal bath ($D_{\text{ne}} = 0$).

Next, we study the dependence of the output power on the nonequilibrium-noise strength D_{ne} using a variable-gain amplifier. We fix the low-pass filter’s cutoff frequency f_{ne} to be ≈ 100 times that of the trap, so that all experiments are in the limit where the nonequilibrium environment provides effectively white-noise fluctuations to the bead. Figure S4(b) shows that the output power increases with the noise strength D_{ne} . At low D_{ne} , the power is that achievable with a purely thermal bath at room temperature. As D_{ne} is increased, the output power increases monotonically. In our experiments, electrochemical reactions at the electrodes limit the maximum achievable noise strength and hence the output power of the information engine. Maximizing both cutoff frequency f_{ne} and noise strength D_{ne} , we achieve an increase of $14\times$ in output power relative to the equilibrium case, to $3.8 \times 10^3 k_{\text{B}}T/s = 1.6 \times 10^{-17}$ W.

A simple scaling argument in the white-noise limit explains the observed performance increase: In Ref. [18], we found the output power of the purely thermal information engine to be, for $t_{\text{s}} \ll 1$ and with $\dot{F}_0 \equiv \dot{F}(D_{\text{ne}} = 0)$,

$$\dot{F}_0 = \sqrt{\frac{2}{\pi}} \delta_{\text{g}} e^{-\delta_{\text{g}}^2/2} \left[1 + \operatorname{erf} \left(\frac{\delta_{\text{g}}}{\sqrt{2}} \right) \right]^{-1}. \quad (6)$$

For $f_{\text{ne}} \gg 1$, the exponentially correlated Ornstein-Uhlenbeck noise $\zeta(t)$ in Eq. (3) becomes effectively white noise, relative to the trap’s cutoff frequency f_{c} . In this limit and ignoring inertial and hydrodynamic corrections to the overdamped Langevin dynamics of the bead [29], it makes sense to view the bead as being immersed in a bath with a higher “effective temperature” T_{ne} . Since ξ and $\tilde{\xi}$ are uncorrelated,

$$\begin{aligned} & \left\langle \left[\xi(t) + \sqrt{D_{\text{ne}}} \tilde{\xi}(t) \right] \left[\xi(t') + \sqrt{D_{\text{ne}}} \tilde{\xi}(t') \right] \right\rangle \\ & = 2(1 + D_{\text{ne}}) \delta(t - t'), \quad (7) \end{aligned}$$

and the effective temperature ratio, in physical units, is $T_{\text{ne}}/T = 1 + D_{\text{ne}}/D$ or, in scaled units, $T_{\text{ne}} = 1 + D_{\text{ne}}$.

The higher effective temperature T_{ne} affects the scaling of output power and, via the length scaling $\sigma(T) =$

$\sqrt{k_{\text{B}}T/\kappa}$, the scaled effective mass,

$$\tilde{\delta}_{\text{g}}(D_{\text{ne}}) = \delta_{\text{g}} \frac{\sigma(1)}{\sigma(1 + D_{\text{ne}})} = \frac{\delta_{\text{g}}}{\sqrt{1 + D_{\text{ne}}}}. \quad (8)$$

Therefore, in the white-noise limit, the output power is

$$\dot{F} = (1 + D_{\text{ne}}) \sqrt{\frac{2}{\pi}} \tilde{\delta}_{\text{g}} e^{-\tilde{\delta}_{\text{g}}^2/2} \left[1 + \operatorname{erf} \left(\frac{\tilde{\delta}_{\text{g}}}{\sqrt{2}} \right) \right]^{-1}. \quad (9)$$

Substituting Eq. (8) for $\tilde{\delta}_{\text{g}}$ into Eq. (9) gives, for $D_{\text{ne}} \gg 1$, the asymptotic behavior $\dot{F} \sim D_{\text{ne}}^{1/2}$ seen in Fig. S4(b).

Finally, we study the dependence of the output power on the scaled mass δ_{g} . Figure 3 shows that for $D_{\text{ne}} = 0$, the output power is maximized at an optimum scaled mass $\delta_{\text{g}} \approx 0.845$ [18]. The optimum arises from a trade-off: having a larger mass increases the gravitational energy gained from a favorable up-fluctuation but reduces the frequency of such fluctuations [18, 30].

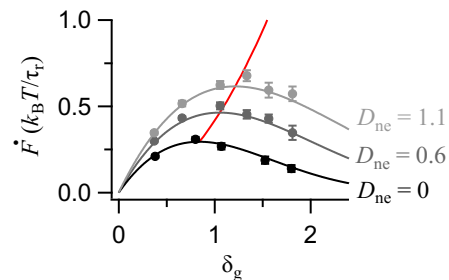


FIG. 3. Optimizing output power as a function of scaled mass δ_{g} for different nonequilibrium-noise strengths. Markers: experiments; lines: Eq. (9). Red curve parametrically plots maximal \dot{F} and δ_{g} that maximizes \dot{F} (calculated from Eq. 10), as functions of D_{ne} .

Figure 3 shows that the optimal mass δ_{g} increases with the nonequilibrium-noise strength D_{ne} . The nonequilibrium noise increases the amplitude of the bead’s fluctuation and makes ratchet events more frequent, thereby shifting the optimal trade-off to higher δ_{g} . Comparing Eqs. (6) and (9), the maximum output power is achieved for $\tilde{\delta}_{\text{g}}(D_{\text{ne}}) \approx 0.845$, and hence, according to Eq. (8), for

$$\delta_{\text{g}} \approx 0.845 \sqrt{1 + D_{\text{ne}}}. \quad (10)$$

Equation (10), the red curve in Fig. 3, represents the maximum achievable output power for different nonequilibrium-noise strengths D_{ne} , achieved at optimal δ_{g} .

Efficiency.—As we have seen, operating an information engine in a nonequilibrium bath with noise strength D_{ne} (and effective temperature T_{ne} in the white-noise limit) can increase output power. At the same time, the

measuring device and controller that gather and exploit the information used to power the engine are in contact with an equilibrium bath at temperature T and thus independent of the nonequilibrium driving force D_{ne} .

We therefore expect the ratio Υ of these two powers (power extracted over minimum operating power), one possible measure of “efficiency,” to increase with D_{ne} . (Note that Υ differs from the Carnot efficiency and, as we will see, is not bounded by unity.) To estimate this increase, we consider the minimum additional work needed to run the controller, which equals the reduction due to the controller’s dynamics in the conditional entropy [31] $H[\Lambda|X]$ of the trap position λ given the particle position x [32]. Therefore the *information power* required to measure, erase information, and control the engine is

$$P_{\text{info}} \equiv \frac{H[\Lambda_{k-1}|X_k] - H[\Lambda_k|X_k]}{t_s}. \quad (11)$$

In the white-noise limit ($f_{\text{ne}} \rightarrow \infty$), the two conditional entropies can be estimated from simulations and analytical approximations (see Appendix). Figure 4(a) compares the input information power P_{info} with the output rate \dot{F} of free-energy gain, Eq. (9), as a function of the noise strength D_{ne} . While the engine output grows as $D_{\text{ne}}^{1/2}$, the input power saturates for large D_{ne} , in principle permitting extraction of orders of magnitude more power than required to run the engine, because larger noise strength offers more fluctuations to rectify but does not affect the controller.

Figure 4(b) shows the engine’s efficiency $\Upsilon \equiv \dot{F}/P_{\text{info}}$, the ratio of output to input powers. With sufficiently strong nonequilibrium fluctuations, output power can exceed input power. In contrast, a “conventional” engine that drags the particle upwards against gravity at the same velocity $v = \dot{F}/\delta_g$ requires trap power $\dot{W} = v^2 + \delta_g v$ and has efficiency < 1 (see Appendix). This conventional strategy is more efficient at low output power, illustrating that rectifying purely thermal fluctuations is inefficient when using a measuring device and controller that operate at the same temperature. However, with sufficiently strong nonequilibrium fluctuations the information ratchet can extract energy more efficiently. Experimentally, we do not reach the regime of larger output than input power; however, with the largest experimental noise strengths, the information ratchet is more efficient than the conventional dragging strategy. Increasing the electric field strengths by using more closely spaced electrodes and more careful choices of electrode material and bath composition could substantially increase the achievable D_{ne} and lead to output powers that exceed minimum information-processing costs.

Discussion and Conclusion.—We have shown experimentally that an information engine in contact with a nonequilibrium bath can extract and store an order of magnitude greater power than it can in the same bath

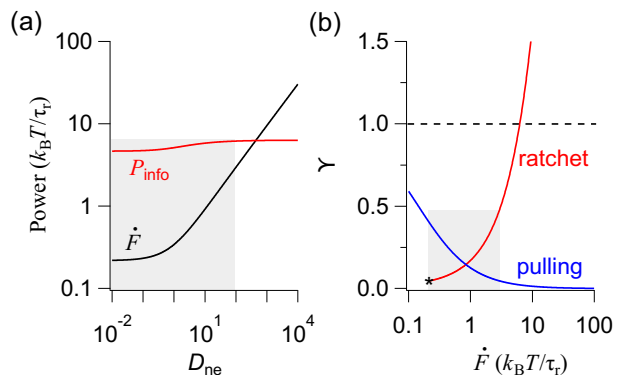


FIG. 4. Numerical estimates of information-engine efficiency in the white-noise limit ($f_{\text{ne}} = 10^4$). (a) Output free-energy gain \dot{F} [Eq. (9)] and information power P_{info} (minimum power to perform measurement, erase information, and control the information engine) as a function of nonequilibrium-noise strength D_{ne} . (b) Efficiency Υ as a function of \dot{F} , compared with a pulling experiment that drags the particle upwards at constant velocity, instead of ratcheting. Star indicates the equilibrium bath, $D_{\text{ne}} = 0$. In all calculations, $\delta_g = 0.38$ and $t_s = 1/40$ (experimental parameters). Shaded regions indicate experimentally accessible nonequilibrium-noise strengths.

without active fluctuations. If the measuring and control devices are at the nominal temperature of the bath (without external forcing) and if the forcing of the nonequilibrium bath is sufficiently strong, then more energy can be extracted than the minimum energy needed to run the measurement-and-control system. Our experiments achieved an efficiency of 48.5%, limited only by the amount of forcing we were able to supply the bath.

To understand the significance of these experimental results, we recall that information engines can be connected to two heat baths, a higher-temperature one for the engine itself and a lower-temperature one for the measuring device and controller [13]. This generalized information engine framework was used recently to automate not only the demon’s function [4] but also its information processing [13]. Such engines can produce net positive work output and, with optimal information processing, have efficiencies that approach the Carnot limit [14]. Similarly, passive ratchets can extract net work only when connected to heat baths at different temperatures [33–35].

As discussed in the Introduction, typical temperature ratios are $\lesssim 10$; however, although an information engine is limited by the Carnot efficiency associated with the ratio of (effective) temperatures of the two baths, it extracts energy from only a very small fraction of modes of the high-temperature bath. In particular, as Fig. S4(a) shows, an engine need only be supplied with modes slightly exceeding f_c (e.g., $f_{\text{ne}} \sim 10^3$ Hz) to achieve half the maximum possible output. By contrast, equipartition implies that a bath in equilibrium at a temperature

T has modes with equal energies up to phonon frequencies, $k_B T/h \approx \mathcal{O}(10^{13})$ Hz, with h Planck’s constant [36]. Thus, the fraction of forced modes is only 10^{-10} . Put another way, if the nonequilibrium forcing is removed and the bath returns to equilibrium, its temperature does not measurably increase.

Engines can thus extract work from nonequilibrium modes, while the associated measuring device remains at equilibrium. Given a white-noise spectrum with frequencies 10–100 \times higher than the engine cutoff frequency, we can assign an effective temperature to the nonequilibrium bath. Because work extraction draws on so few modes, the effective temperature of the bath can be orders of magnitude higher than physical temperatures.

Very high effective temperature and correspondingly large work-extraction rates are implicit in many old technologies: Sailboats move because their sails are constantly adjusted to catch the wind, and wind turbines similarly generate power by adjusting their rotors to be normal to the fluctuating wind direction [37]. On a smaller scale, self-winding watches, first developed in the 18th century [38], rectify the nonequilibrium fluctuations supplied by movements of the wearer’s arm [35]. More recent experimental realizations include ratchets driven by granular gasses [39–43] that achieve effective temperatures up to $10^{15}\times$ room temperature [44–46] and rotors driven by turbulence [47].

In the above examples, the scale of the system correlates with the power extracted. Our experiments use micron-scale beads and extract powers of $2.97 k_B T/\tau_r \approx 10^{-17}$ W. For granular media, millimeter-sized beads lead to extracted powers of 10^{-6} W [43]. For wind turbines, the 100-m scale blades lead to extracted powers of 10^6 W [48]. Thus, larger length scales increase the power that can be extracted from a fluctuating environment.

Nonequilibrium fluctuations can also be generated by active media [49–63] such as (suspensions of) microswimmers [64] and active Brownian particles [65]. The vastly higher values of effective temperature that one can achieve relative to physical temperatures suggest the potential for drastic efficiency increases. Indeed, we have seen that the work extracted can in principle exceed the minimum information costs associated with the engine function. We then speculate that exploitation of fluctuations, as shown here, could be an organizing principle for molecular machinery, where strong nonequilibrium fluctuations [66, 67] have been shown to speed up various cellular processes [68, 69].

Finally, our results also highlight a different way to understand energy harvesting [70–73] by microscopic devices. Such analyses are often specific to the type of systems analyzed. For example, mechanical energy harvesters depend heavily on resonant-forcing mechanisms that make inefficient use of the spectrum of fluctuations [74]. Our approach gives maximum estimates (for a given fluctuation spectrum) of the power that can in prin-

ciple be extracted and can thus serve as benchmarks for existing systems and may suggest new extraction strategies. The question, which has only begun to be addressed in special cases, is whether “intelligently chosen interventions” [75] can outperform standard passive rectification strategies, such as full-wave rectifier bridge circuits based on diodes or Brownian ratchets [76].

We thank Joseph Lucero for helpful conversations. This research was supported by grant FQXi-IAF19-02 from the Foundational Questions Institute Fund, a donor-advised fund of the Silicon Valley Community Foundation. Additional support was from grant FQXi-RFP-1820, co-sponsored with the Fetzer Franklin Fund (S.S.), Natural Sciences and Engineering Research Council of Canada (NSERC) Discovery Grants (D.A.S. and J.B.) and a Tier-II Canada Research Chair (D.A.S.).

APPENDIX

Experimental Apparatus

Figure S1 shows the schematic diagram of the apparatus. A bead is trapped by focusing a horizontally aligned (perpendicular to gravity) green trapping laser (HÜBNER Photonics, Cobolt Samba, 1.5 W, 532 nm), using a microscope objective (MO1, water-immersion 60 \times Olympus objective 1.2 NA).

A red laser (HÜBNER Photonics, Cobolt Flamenco, 100 mW, 660-nm) is used for bead-position detection. The scattered detection light from the bead is collected using another microscope objective (MO2, 40 \times Nikon, 0.5 NA) and focused on the quadrant photo-diode (QPD, First Sensor, QP50-6-18u-SD2) to measure the bead position. The position of the trap is changed using acousto-optic deflectors (AODs, DTSXY-250-532, AA Opto Electronic), one for each axis perpendicular to the direction of laser propagation. We use the AOD that controls the axis parallel to gravity, pointing out-of-plane, to perform the experiments. References [18, 77] provide more details about the apparatus and the calibration.

Nonequilibrium noise source

The nonequilibrium energy is generated by connecting the sample chamber to an external electronic-noise source. The sample chamber was built using a glass slide and a coverslip, which were separated by double-layered sticky copper tape. Long strips of copper tape extend beyond the glass slide and connect to external electrodes using alligator clips (see Fig. S1, orange inset). The space between the electrodes is ≈ 5 mm.

To generate the stochastic forces, we use the Johnson noise of a 300-k Ω resistor (TeachSpin, Noise Fundamentals). The TeachSpin noise source has a built-in, two-

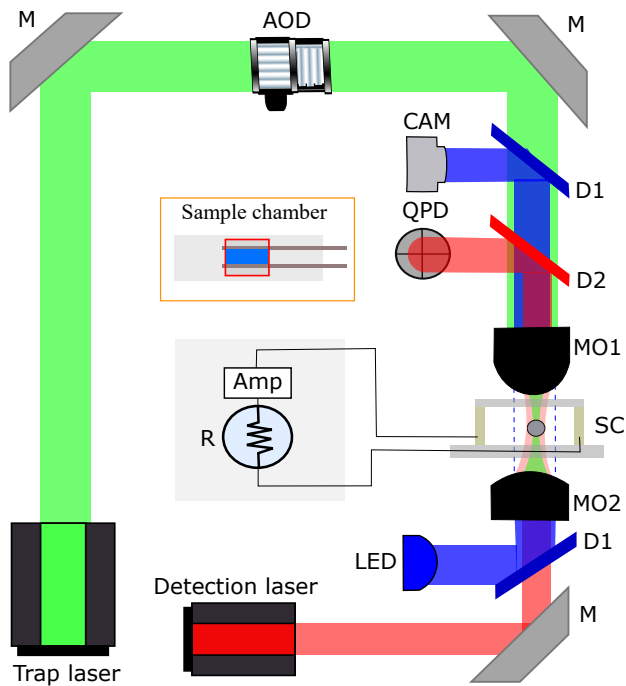


FIG. S1. Schematic diagram of the experimental apparatus with external electrical noise (shaded gray region). R = resistor, Amp = amplifier, M = mirror, AOD = acousto-optic deflector, D1 = blue dichroic filter, D2 = red dichroic filter, SC = sample chamber, MO1 = trapping microscope objective, and MO2 = detection microscope objective. Inset (orange box): sample chamber with two copper-tape electrodes (brown lines). The blue shaded region represents the bead solution.

stage preamplifier whose overall gain is $G_1 = 600$. The noise is further amplified using two other external amplifiers: First, there is a variable-gain amplifier ($G_2 = 10\text{--}10^4$) using a TeachSpin noise controller. Second, there is a home-built, fixed-gain ($G_3 = 15$) amplifier that can source the higher current that is needed for this experiment (the two copper electrodes form a capacitor that charges more quickly with higher currents).

We control the bandwidth of the noise using high-pass and low-pass two-pole Butterworth filters included with the TeachSpin controller. The high-pass filter cutoff frequency is set to 10 Hz to prevent electroconvection in the fluid and low-frequency electronic noise. Its bandwidth is sufficiently small compared to the cutoff frequency of the nonequilibrium noise (24 kHz) that calculations of fluctuation strengths that extend to zero frequency do not differ significantly from the experimental results. Experiments at the lowest three cutoff frequencies (10, 30 and 100 Hz) in Fig. 2 (a) were performed using the built-in high-pass filter of the TeachSpin amplifier with cutoff frequency of 2.5 Hz.

The power spectra of trapped beads at different low-pass frequency cutoff and amplifier gain are presented in

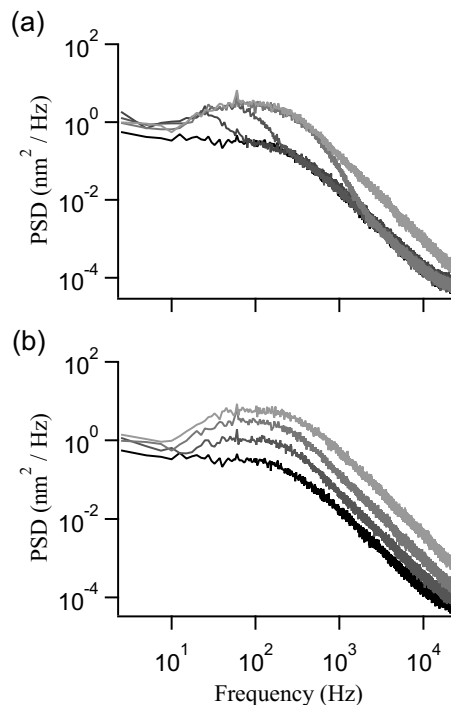


FIG. S2. Power spectral density of a trapped bead in the presence of external noise. Black curve: power spectrum in the absence of nonequilibrium noise. (a) Lighter shades of gray: fixed noise amplitude (variable-amplifier gain $G_2 = 6 \times 10^2$) at higher cutoff frequencies of the noise: 30, 100, 1000, and 100 000 Hz. (b) Lighter shades of gray: fixed cutoff frequency (100 000 Hz) with increasing variable-amplifier gain, with $G_2 = \{3, 6, 10\} \times 10^2$.

Fig. S2 (a) and (b), respectively. Experiments were performed for parameter values that did not generate electrochemical breakdown of the electrodes. The copper-tape electrodes were used for simplicity; replacing them with platinum electrodes would increase the range of voltages that can be applied to the bead.

In Fig. S3, we show the power spectral densities of the background electronic noise (black, using a 1Ω resistor, whose Johnson noise is negligible relative to the amplifier noise) and $300\text{-k}\Omega$ resistor (red, with the background noise). The high-pass and low-pass filter values were 10 and 100 000 Hz, respectively. The latter low-pass cutoff frequency (100 kHz) is higher than the cutoff frequency of the nonequilibrium noise (24 kHz) and thus does not play a significant role in determining the overall noise properties. The signals were measured using all the amplifiers, with nominal amplifications $G_1 = 600$, $G_2 = 10$, and $G_3 = 15$. The sampling frequency was 400 kHz. The measured output signals were referred back to the respective noise sources by dividing the PSD responses by $(G_1 G_2 G_3)^2$.

The blue curve represents the background-subtracted power spectral density (PSD) of the $300\text{-k}\Omega$ resistor. The

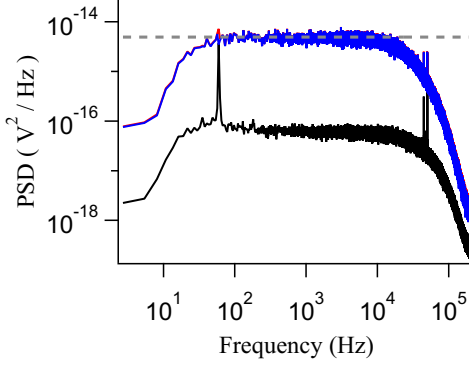


FIG. S3. Amplifier noise characterization. Power spectral density of the electronic noise (black), and 300-k Ω resistor with (red) and without (blue) the background electronic noise. Note that the red curve is almost covered by the blue one. Gray dashed line: expected Johnson noise, for $T = 298$ K and $R = 300$ k Ω .

gray line represents the expected Johnson noise spectral density ($= 4 k_B T R$) for a 300-k Ω resistor, calculated using $R = 300$ k Ω and $T = 298$ K. We find that experimentally measured response (blue) and expected noise (gray line) are in good agreement. The empirical low- and high-frequency cutoffs are defined as the frequencies where the measured power is reduced by a factor of 1/2. We find 18 Hz and 24 kHz, respectively.

We measure the signal-to-noise ratio (SNR) using the PSDs, where the signal is the Johnson noise of the 300-k Ω resistor and the noise is the background electronic noise. We fit the flat regions of the power spectral densities

(black and blue curves) to constants and find from the ratio of the fit values that $\text{SNR} \approx 76.8$.

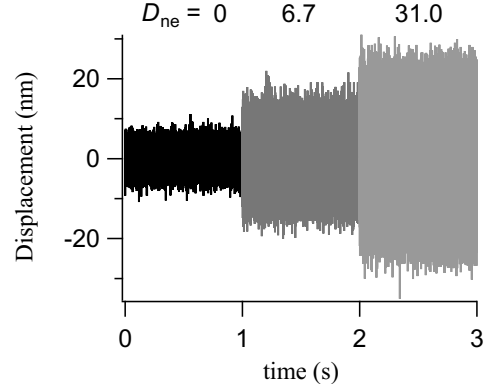


FIG. S4. Displacement of the bead ($x_{k+1} - x_k$) in a static trap for $D_{\text{ne}} = 0, 6.7,$ and 31.0 .

Numerical simulations

We simulate the dynamics of the engine with non-equilibrium fluctuations using discrete-time dynamics to model the evolution of the bead and the nonequilibrium noise from one time step to the next. To this end, we integrate over one time step the coupled Langevin equations for the bead x [Eq. (1)] and for the nonequilibrium noise ζ [Eq. (3)]. Then the new particle position x_{k+1} and the next value of the noise ζ_{k+1} are drawn from a bivariate Gaussian distribution $\mathcal{N}(\mathbf{r}; \boldsymbol{\mu}, \boldsymbol{\Sigma})$ in \mathbf{r} with mean $\boldsymbol{\mu}$ and covariance matrix $\boldsymbol{\Sigma}$. Here,

$$p(x_{k+1}, \zeta_{k+1} | x_k, \zeta_k) = \mathcal{N} \left[\begin{pmatrix} x_{k+1} \\ \zeta_{k+1} \end{pmatrix}; \begin{pmatrix} \mu_{x_{k+1}}(x_k, \zeta_k) \\ e^{-f_{\text{ne}} t_s} \zeta_k \end{pmatrix}, \begin{pmatrix} c_{xx} & c_{x\zeta} \\ c_{x\zeta} & c_{\zeta\zeta} \end{pmatrix} \right] \quad (\text{S1})$$

with mean

$$\mu_{x_{k+1}}(x_k, \zeta_k) = (x_k - \lambda_k + \delta_g) e^{-t_s} + \lambda_k - \delta_g + \zeta_k \frac{1}{1 - f_{\text{ne}}} (e^{-f_{\text{ne}} t_s} - e^{-t_s}), \quad (\text{S2})$$

and covariances

$$c_{xx} = \frac{4D_{\text{ne}}f_{\text{ne}}^2}{(1 - f_{\text{ne}})^2(1 + f_{\text{ne}})} e^{-(1+f_{\text{ne}})t_s} - \frac{D_{\text{ne}}f_{\text{ne}}}{(1 - f_{\text{ne}})^2} e^{-2f_{\text{ne}}t_s} - \frac{D_{\text{ne}}f_{\text{ne}}^2 + (1 - f_{\text{ne}})^2}{(1 - f_{\text{ne}})^2} e^{-2t_s} + \frac{1 + D_{\text{ne}}f_{\text{ne}} + f_{\text{ne}}}{1 + f_{\text{ne}}} \quad (\text{S3a})$$

$$c_{x\zeta} = D_{\text{ne}} \left[\frac{2f_{\text{ne}}^2}{1 - f_{\text{ne}}^2} e^{-(1+f_{\text{ne}})t_s} - \frac{f_{\text{ne}}}{1 - f_{\text{ne}}} e^{-2f_{\text{ne}}t_s} + \frac{f_{\text{ne}}}{1 + f_{\text{ne}}} \right] \quad (\text{S3b})$$

$$c_{\zeta\zeta} = D_{\text{ne}}f_{\text{ne}} (1 - e^{-2f_{\text{ne}}t_s}), \quad (\text{S3c})$$

Equation (S1) was used to simulate the relaxation of the bead in a static potential at λ_k and the evolution of

the additional Ornstein-Uhlenbeck noise. The trap was

updated according to

$$\lambda_k = \lambda_{k-1} + 2\Theta(x_k - \lambda_{k-1})(x_k - \lambda_{k-1}), \quad (\text{S4})$$

where $\Theta(\cdot)$ denotes the Heaviside step function.

To obtain the curve in Fig. 2, the rate of free-energy gain $\dot{F} = \Delta F/Kt_s = \delta_g(\lambda_K - \lambda_0)/Kt_s$ from $K = 10^4$ time steps was averaged over 10^4 runs. One initial run was used to reach steady-state ratcheting operation.

Nonequilibrium noise strength

Here we discuss the method used to determine experimentally the strength D_{ne} of the nonequilibrium noise source. The measurements are done independently from the information-engine experiments. We determine D_{ne} by measuring the variance of bead displacements $\Delta x := x_{k+1} - x_k$ in a static trap in a bath with nonequilibrium-noise cutoff frequency ($f_{\text{ne}} = 24$ kHz); see Fig. S3. At that frequency the bead essentially experiences white-noise fluctuations, such that (in scaled units) $\text{Var}(\Delta x) \approx (1 + D_{\text{ne}})(1 - e^{-t_s})$, which in principle permits determination of D_{ne} .

To also account for small corrections arising from the finite frequency of the nonequilibrium noise, we calculate the full expression for the variance of bead displacements. The dynamics of the bead in a static trap with nonequilibrium noise are given by the propagator in Eq. (S1) and setting $\delta_g = \lambda_k = 0$. Specifically,

$$p(x_{k+1}|x_k, \zeta_k) = \mathcal{N}[x_{k+1}; \mu_{x_{k+1}}(x_k, \zeta_k), c_{xx}], \quad (\text{S5})$$

a Gaussian with mean $\mu_{x_{k+1}}(x_k, \zeta_k)$ and variance c_{xx} given by Eqs. (S2) and (S3a), respectively.

From Eq. (S1) we also obtain the stationary probability distribution by taking the limit $t_s \rightarrow \infty$,

$$\pi(x_k, z_k) = \mathcal{N}\left[\begin{pmatrix} x_k \\ \zeta_k \end{pmatrix}; \begin{pmatrix} 0 \\ 0 \end{pmatrix}, \begin{pmatrix} 1 + \frac{D_{\text{ne}}f_{\text{ne}}}{1+f_{\text{ne}}} & \frac{D_{\text{ne}}f_{\text{ne}}}{1+f_{\text{ne}}} \\ \frac{D_{\text{ne}}f_{\text{ne}}}{1+f_{\text{ne}}} & D_{\text{ne}}f_{\text{ne}} \end{pmatrix}\right]. \quad (\text{S6})$$

The distribution of the increment given x_k and ζ_k reads

$$p(\Delta x|x_k, \zeta_k) = \mathcal{N}[\Delta x; \mu_x(x_k, \zeta_k) - x_k, c_{xx}]. \quad (\text{S7})$$

Averaging this distribution over the stationary distribution of x_k and ζ_k in Eq. (S6) yields the average variance

of the increment,

$$\begin{aligned} \text{Var}(\Delta x) &= (e^{-t_s} - 1)^2 \left(1 + \frac{D_{\text{ne}}f_{\text{ne}}}{1+f_{\text{ne}}}\right) \\ &\quad + 2\frac{(e^{-t_s} - 1)}{1-f_{\text{ne}}} (e^{-f_{\text{ne}}t_s} - e^{-t_s}) \frac{D_{\text{ne}}f_{\text{ne}}}{1+f_{\text{ne}}} \\ &\quad + \left[\frac{1}{1-f_{\text{ne}}} (e^{-f_{\text{ne}}t_s} - e^{-t_s})\right]^2 D_{\text{ne}}f_{\text{ne}} + c_{xx} \end{aligned} \quad (\text{S8a})$$

$$\begin{aligned} &= \frac{2f_{\text{ne}}D_{\text{ne}}}{f_{\text{ne}}^2 - 1} (f_{\text{ne}} - 1 - f_{\text{ne}}e^{-t_s} + e^{-f_{\text{ne}}t_s}) \\ &\quad + 2(1 - e^{-t_s}). \end{aligned} \quad (\text{S8b})$$

The increase of bead displacement variance relative to the equilibrium case thus reads

$$\frac{\text{Var}(\Delta x)}{\text{Var}_0(\Delta x)} = 1 + D_{\text{ne}} \frac{f_{\text{ne}}(f_{\text{ne}} - 1 - f_{\text{ne}}e^{-t_s} + e^{-f_{\text{ne}}t_s})}{(f_{\text{ne}}^2 - 1)(1 - e^{-t_s})}. \quad (\text{S9})$$

Equation (S9) was used to estimate D_{ne} in experiments, where the typical parameter values were $t_s = 20 \mu\text{s} / \tau_r = 0.025$ and $f_{\text{ne}} = 24 \text{ kHz} / f_c = 118$. Note that, in the white-noise limit where $f_{\text{ne}} \gg 1$, the right-hand side of Eq. (S9) reduces to $1 + D_{\text{ne}}$, indicating that the position increments result from white-noise fluctuations with a higher effective temperature, in agreement with Eq. (7) in the main text.

Information efficiency

Reference [32] shows that to carry out feedback control, a work W_k^{add} is needed in addition to the trap work. With no nonequilibrium noise ($D_{\text{ne}} = 0$) and for feedback rules that are independent of the current controller state, i.e., rules of the form $p_c(z_k|x_k)$, with z_k the state of the feedback controller, the additional work is no less than the change in entropy achieved by the control operation,

$$W_k^{\text{add}} \geq k_{\text{B}}T (H[Z_{k-1}|X_k] - H[Z_k|X_k]) \quad (\text{S10a})$$

$$= k_{\text{B}}T (H[X_k, Z_{k-1}] - H[X_k, Z_k]) \quad (\text{S10b})$$

$$=: -k_{\text{B}}T \Delta H_k^Z, \quad (\text{S10c})$$

where T is the temperature of the feedback-controlled system and the controller, and ΔH_k^Z is the change in joint entropy [31, Chap. 2.2] due to the dynamics of the controller Z .

Our information engine differs from the description in Ref. [32] in two ways: First, the particle (but not the controller) is subjected to additional colored nonequilibrium noise whose exponential correlation leads to long-time correlations between particle positions, thus violating the Markov assumption. Second, the feedback rule (S4) is *recursive*: the next trap position λ_k depends not only on

the current particle position x_k but also on the current trap position λ_{k-1} .

The first difference is addressed by focusing on the white-noise limit of the nonequilibrium noise, $f_{\text{ne}} \rightarrow \infty$, thus ensuring Markovian particle dynamics at an effective temperature T_{ne} which is higher than the temperature T of the controller. The second difference does not impact the minimum additional work in Eqs. (S10), as we show below.

Recursive controller architecture

Reference [32] shows that Eq. (S10) is saturated by a control protocol that quasistatically and reversibly carries the conditional controller state from the distribution before the controller update, $p(z_{k-1}|x_k)$, to the distribution after the controller update, $p(z_k|x_k)$, by choosing a time-dependent control potential for the controller state Z such that the conditional controller distributions correspond to the equilibrium distribution under the control potential at the beginning and end of the controller update. The update can be made arbitrarily short yet still reversible when the controller mobility during the update is large.

Here we require recursive controller updates $p_c(z_k|x_k, z_{k-1})$. The protocol of Ref. [32] cannot be applied directly because, during its update to $p_c(z_k|x_k)$, all memory of the previous controller state z_{k-1} was lost; however, this can be remedied by adding a temporary auxiliary variable u to the controller, as follows: Starting out in an uncorrelated reference state, the controller state z_{k-1} is copied to the auxiliary variable u . Next, the controller update is carried out as described in Ref. [32] with u taking the role of the previous controller state z_{k-1} : $p_c(z_k|x_k, z_{k-1} = u)$. Finally, the auxiliary variable is reset to the initial uncorrelated reference state. Reference [78] argues that such auxiliary, or hidden, variables are generally necessary when implementing computations with Markovian dynamics.

As in Ref. [32], all steps are carried out quasistatically and reversibly, such that the total heat flow equals the total change in joint entropy,

$$\Delta H_k^Z := H[X_k, Z_k] + H_{\text{ref}}[U] - (H[X_k, Z_{k-1}] + H_{\text{ref}}[U]) \quad (\text{S11a})$$

$$= H[X_k, Z_k] - H[X_k, Z_{k-1}], \quad (\text{S11b})$$

where $H_{\text{ref}}[U]$ is the entropy of the auxiliary variable's reference state. Consequently, the additional work needs to at least compensate the decrease in joint entropy by the controller.

For our information ratchet, a minimal model of the controller state z_k is simply the trap position λ_k . Using rescaled units and dividing by the sampling time t_s

gives the lower bound for the *additional power* required to update the trap position,

$$P_{\text{info}} := -\frac{H[X_k, \Lambda_k] - H[X_k, \Lambda_{k-1}]}{t_s} \quad (\text{S12a})$$

$$= \frac{H[\Lambda_{k-1}|X_k] - H[\Lambda_k|X_k]}{t_s}, \quad (\text{S12b})$$

which we call *information power*, since it is defined purely in terms of the information gathered through the operation of feedback control. It represents the minimum additional power that must be supplied to the engine to make the feedback step thermodynamically consistent. The real experimental equipment dissipates orders of magnitude more power than this lower bound; however, this need not deter us from studying the fundamental limits of this information engine.

Steady-state ratcheting

To evaluate Eq. (S12b), we require the conditional distributions $p(\lambda_{k-1}|x_k)$ before the trap update and $p(\lambda_k|x_k)$ after the trap update.

We use the fact that, after many feedback steps, the distributions of the *relative coordinates*

$$r_k := \lambda_k - x_k \quad (\text{S13a})$$

$$r_k^- := \lambda_{k-1} - x_k \quad (\text{S13b})$$

become stationary, i.e.,

$$p(\lambda_k|x_k) = p(r_k + x_k|x_k) \rightarrow \pi(r_k) \quad (\text{S14a})$$

$$p(\lambda_{k-1}|x_k) = p(r_k^- + x_k|x_k) \rightarrow \pi^-(r_k^-). \quad (\text{S14b})$$

This allows us to rewrite the conditional entropy

$$H[\Lambda_k|X_k] = -\int dx_k \int d\lambda_k p(x_k, \lambda_k) \ln p(\lambda_k|x_k) \quad (\text{S15a})$$

$$= -\int d\lambda_k p(\lambda_k) \int dr_k \pi(r_k) \ln \pi(r_k) \quad (\text{S15b})$$

$$= -\int dr_k \pi(r_k) \ln \pi(r_k) \quad (\text{S15c})$$

$$=: H[R_k], \quad (\text{S15d})$$

in terms of the entropy of the relative variable, $H[R_k]$, and similarly for

$$H[\Lambda_{k-1}|X_k] = -\int dr_k \pi^-(r_k^-) \ln \pi^-(r_k^-) \quad (\text{S16a})$$

$$=: H[R_k^-]. \quad (\text{S16b})$$

Approximations for steady-state relative distributions

It remains to determine the stationary distributions $\pi(r)$ and $\pi^-(r^-)$ for which, unfortunately, no closed-form

solutions exist. We can, however, approximate them to low order in the sampling time t_s .

With feedback sufficiently fast, every fluctuation over the threshold is immediately caught and the trap moved in response such that the relative coordinate is reflected to the other side of the threshold. Hence, the dynamics relative to the trapping potential can be approximated by diffusion with a reflecting boundary at $r = 0$, which has the stationary distribution

$$\pi(r) = \begin{cases} A \exp\left[-\frac{(r-\delta_g)^2}{2(1+D_{ne})}\right] & r \geq 0 \\ 0 & r < 0 \end{cases}, \quad (\text{S17})$$

i.e., the equilibrium distribution at relative temperature $1 + D_{ne}$ but truncated at $r = 0$. Normalization implies

$$A = \sqrt{\frac{2}{\pi(1+D_{ne})}} \left[1 + \operatorname{erf}\left(\frac{\delta_g}{\sqrt{2(1+D_{ne})}}\right) \right]^{-1}. \quad (\text{S18})$$

This approximation holds to leading order in the sampling time t_s , as we now demonstrate.

The dynamics in Eq. (1) of the main text in the white-noise ($f_{ne} \rightarrow \infty$) limit lead to the propagator

$$p_x(x_{k+1}|x_k, \lambda_k) = \mathcal{N}\left[x_{k+1}; \mu_x(x_k, \lambda_k; t_s), c(t_s)\right], \quad (\text{S19})$$

a Gaussian with mean

$$\mu_x(x_k, \lambda_k; t_s) = (x_k - \lambda_k) e^{-t_s} + \lambda_k - (1 - e^{-t_s}) \delta_g \quad (\text{S20})$$

and variance

$$c(t_s) = (1 + D_{ne})(1 - e^{-2t_s}). \quad (\text{S21})$$

In relative coordinates,

$$p_r(r^-|r) = \mathcal{N}\left[r^-; r e^{-t_s} + (1 - e^{-t_s}) \delta_g, c(t_s)\right]. \quad (\text{S22})$$

Thus, the stationary distribution before feedback is

$$\pi^-(r^-) = \int dr p_r(r^-|r) \pi(r) \quad (\text{S23a})$$

$$= \frac{A}{2} \exp\left[-\frac{(r^- - \delta_g)^2}{2(1+D_{ne})}\right] \times \left\{ 1 - \operatorname{erf}\left[\frac{(\delta_g - r^-) e^{-t_s} - \delta_g}{\sqrt{2(1+D_{ne})(1 - e^{-2t_s})}}\right] \right\}. \quad (\text{S23b})$$

In relative coordinates the feedback rule (S4) is

$$r = r^- - 2r^- \Theta(r^-). \quad (\text{S24})$$

This amounts to reflecting the negative tail of the distribution $\pi^-(r^-)$ about $r^- = 0$, giving, for $r^- > 0$ and to

leading order in t_s ,

$$\begin{aligned} \pi^-(r) + \pi^-(-r) &= \frac{A}{2} \exp\left[-\frac{(r^- - \delta_g)^2}{2(1+D_{ne})}\right] \\ &\times \left[2 - \operatorname{erf}\left(\frac{r}{\sqrt{2(1+D_{ne})t_s}}\right) \right. \\ &\left. + \operatorname{erf}\left(\frac{r}{\sqrt{2(1+D_{ne})t_s}}\right) \right] \quad (\text{S25a}) \\ &= \pi(r). \quad (\text{S25b}) \end{aligned}$$

Thus, reflecting the stationary distribution recovers the truncated Gaussian in Eq. (S17).

With these approximations, we recover the correct rate of free-energy gain for $t_s \rightarrow 0$. Using the fact that $\lambda_k = \lambda_{k-1} + 2(x_k - \lambda_{k-1})$ if $x_k - \lambda_{k-1} > 0$, we get

$$\dot{F} = \frac{\delta_g}{t_s} \int_{-\infty}^{x_k} d\lambda_{k-1} 2(x_k - \lambda_{k-1}) p(\lambda_{k-1}|x_k) \quad (\text{S26a})$$

$$= -\frac{2\delta_g}{t_s} \int_{-\infty}^0 dr^- r^- \pi^-(r^-). \quad (\text{S26b})$$

For small t_s , the left tail of $\pi^-(r^-)$ is dominated by the contribution from the error function in Eq. (S23b), giving

$$\begin{aligned} \pi^-(r^-) &\approx \frac{A}{2} \exp\left[-\frac{\delta_g^2}{2(1+D_{ne})}\right] \\ &\times \left\{ 1 - \operatorname{erf}\left[\frac{(\delta_g - r^-) e^{-t_s} - \delta_g}{\sqrt{2(1+D_{ne})(1 - e^{-2t_s})}}\right] \right\} \quad (\text{S27}) \end{aligned}$$

and thus

$$\dot{F} \xrightarrow{t_s \rightarrow 0} (1 + D_{ne}) A \exp\left[-\frac{\delta_g^2}{2(1+D_{ne})}\right]. \quad (\text{S28})$$

Together with A from Eq. (S18), this is Eq. (9) of the main text, which itself originates from Ref. [18], where it was calculated for $D_{ne} = 0$ using a different method based on mean first-passage times.

We use $\pi(r)$ [Eq. (S17)] to numerically evaluate $H[R_k]$ [Eq. (S15b)] and $\pi^-(r^-)$ [Eq. (S23b)], then numerically calculate $H[R_k^-]$ [Eq. (S16a)], and finally evaluate P_{info} in Eq. (S12b).

We compare the information power calculated from approximations of the stationary distribution with that calculated from sampled distributions using numerical simulations according to Sec. . Using 10^4 feedback steps to reach the steady-state regime, we estimated the distributions $\pi(r_k)$ and $\pi(r_k^-)$ from $K = 10^6$ feedback steps using histograms with $n = 10^2$ bins of uniform width. The entropy was then computed as

$$H[R_k] = -\sum_{i=1}^n \frac{n_i}{K} \ln\left(\frac{n_i}{K dr}\right), \quad (\text{S29})$$

where n_i is the number of samples in the i th bin. We similarly estimated $H[R_k^-]$. (This histogram method of estimating entropy is systematically biased [79, App. A.8]; however, the bias is insignificant due to the large number of samples and vanishes upon taking the difference of two similarly estimated entropies.)

Figure S5(a) shows the information power as a function of the nonequilibrium-noise strength D_{ne} . The approximation matches the estimate from simulations.

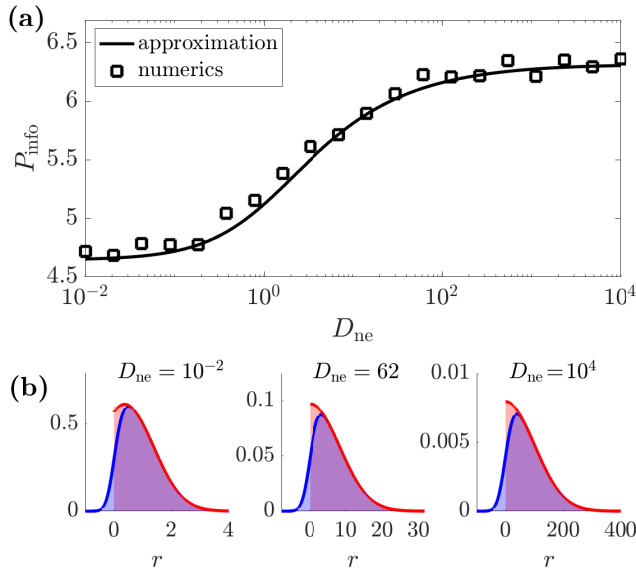


FIG. S5. Information power P_{info} and distributions of relative coordinate. (a) Information power (S12b) as a function of nonequilibrium-noise strength D_{ne} . Curve: numerical evaluation of Eqs. (S15b) and (S16a) using the analytic approximations in Eqs. (S17) and (S23b). Symbols: numerical simulation (Sec.). (b) Stationary relative distributions $\pi(r)$ after feedback (red) and $\pi^-(r^-)$ before feedback (blue), for different nonequilibrium-noise strengths D_{ne} . Curves: analytic approximations [Eqs. (S17) and (S23b)]. Shaded areas: numerical simulations. Parameters are $t_s = 1/40$, $\delta_g = 0.38$, and $f_{\text{ne}} = 10^4$.

Interestingly, the information power saturates in the limit of strong nonequilibrium noise, $D_{\text{ne}} \rightarrow \infty$: In this limit, the stationary distributions have a generic shape with a width scaled by the nonequilibrium-noise strength D_{ne} [see Fig. S5(b)]. To see this explicitly, consider the

limit $D_{\text{ne}} \gg 1$ in Eqs. (S17) and (S23b),

$$\pi(r) \rightarrow \begin{cases} \sqrt{\frac{2}{\pi D_{\text{ne}}}} \exp\left[-\frac{1}{2}\left(\frac{r}{\sqrt{D_{\text{ne}}}}\right)^2\right], & r \geq 0 \\ 0, & r < 0 \end{cases} \quad (\text{S30a})$$

$$= \pi(r/\sqrt{D_{\text{ne}}}) \quad (\text{S30b})$$

$$\pi^-(r^-) = \frac{A}{2} \exp\left[-\frac{(r^-)^2}{2D_{\text{ne}}}\right] \quad (\text{S30c})$$

$$\times \left\{ 1 + \operatorname{erf}\left[\frac{r^- e^{-t_s}}{\sqrt{2D_{\text{ne}}(1 - e^{-2t_s})}}\right] \right\} \\ = \pi^-(r^-/\sqrt{D_{\text{ne}}}). \quad (\text{S30d})$$

Scaling the width of a distribution by a factor a , while keeping it normalized, results in an entropy increase of $\ln|a|$ [31, Chap. 8.6]. Since this scaling affects both distributions $\pi(r)$ and $\pi^-(r^-)$, the entropy difference in Eq. (S12b) remains unchanged, resulting in saturating information power for $D_{\text{ne}} \rightarrow \infty$.

Figure 4(a) in the main text compares the input information power P_{info} with the output free-energy gain \dot{F} for different nonequilibrium-noise strengths D_{ne} . When the noise is purely thermal, the costs of running the information engine exceed the benefit gained from extracting thermal fluctuations, in accordance with the second law. However, when the nonequilibrium environment supplies sufficiently large fluctuations, the output can dwarf the input by orders of magnitude.

Comparison to raising the particle without feedback

We contrast the information power necessary to run the information engine with the trap power required to drag the particle upwards without feedback. The equation of motion of the particle position x in a trap that is moved upwards at velocity v is

$$\dot{x} = -[x - \lambda(t)] - \delta_g + \xi(t) + \zeta(t), \quad (\text{S31})$$

where $\lambda(t) = vt$ is the time-dependent trap position, and $\xi(t)$ and $\zeta(t)$ are the zero-mean thermal white noise and zero-mean nonequilibrium colored noise, respectively (see main text).

Then, the rate of work done on the particle (the trap power) is

$$\dot{W} = \left\langle \partial_\lambda \left\{ \frac{1}{2} [x - \lambda(t)]^2 \right\} \dot{\lambda}(t) \right\rangle \quad (\text{S32a})$$

$$= -v \langle x - \lambda(t) \rangle \quad (\text{S32b})$$

$$= v^2 + v \delta_g, \quad (\text{S32c})$$

where we used the average of Eq. (S31) in line (S32c), $v = \langle \dot{x} \rangle = -\langle [x - \lambda(t)] \rangle - \delta_g$.

With $\dot{F} = v\delta_g$, we compare the efficiency of the information engine with that of a feedback-free pulling strategy that achieves the same output power:

$$\dot{W} = \dot{F} + \frac{\dot{F}^2}{\delta_g^2} \quad (\text{S33a})$$

$$> \dot{F}, \quad (\text{S33b})$$

which indicates that the efficiency is bounded by one, $\dot{F}/\dot{W} < 1$. Figure 4(b) in the main text compares the efficiencies of both driving strategies. In contrast to the feedback-free pulling strategy, the information engine can have efficiency (or coefficient of performance) far greater than one.

Simulation code and data

The code used to perform the simulations and to generate the numerical data can be found in Ref. [80].

* These authors contributed equally.

- [1] J. C. Maxwell, *Theory of Heat*, 3rd ed. (Longmans, Green, and Co., 1872).
- [2] H. Leff and A. F. Rex, *Maxwell's Demon 2: Entropy, Classical and Quantum Information, Computing* (CRC Press, 2002).
- [3] J. M. Parrondo, J. M. Horowitz, and T. Sagawa, Thermodynamics of information, *Nat. Phys.* **11**, 131 (2015).
- [4] L. Szilard, On the decrease in entropy in a thermodynamic system by the intervention of intelligent beings, in *Maxwell's Demon 2*, edited by H. S. Leff and A. F. Rex (IOP Publishing, 2003).
- [5] S. Toyabe, T. Sagawa, M. Ueda, E. Muneyuki, and M. Sano, Experimental demonstration of information-to-energy conversion and validation of the generalized Jarzynski equality, *Nat. Phys.* **6**, 988 (2010).
- [6] J. V. Koski, V. F. Maisi, J. P. Pekola, and D. V. Averin, Experimental realization of a Szilard engine with a single electron, *Proc. Natl. Acad. Sci. U.S.A.* **111**, 13786 (2014).
- [7] K. Chida, S. Desai, K. Nishiguchi, and A. Fujiwara, Power generator driven by Maxwell's demon, *Nat. Commun.* **8**, 1 (2017).
- [8] G. Paneru, D. Y. Lee, T. Tlusty, and H. K. Pak, Lossless Brownian information engine, *Phys. Rev. Lett.* **120**, 020601 (2018).
- [9] M. Ribezzi-Crivellari and F. Ritort, Large work extraction and the Landauer limit in a continuous Maxwell demon, *Nat. Phys.* **15**, 660 (2019).
- [10] N. Cottet, S. Jezouin, L. Bretheau, P. Campagne-Ibarcq, Q. Ficheux, J. Anders, A. Auffèves, R. Azouit, P. Rouchon, and B. Huard, Observing a quantum Maxwell demon at work, *Proc. Natl. Acad. Sci. U.S.A.* **114**, 7561 (2017).
- [11] C. H. Bennett, The thermodynamics of computation—a review, *Int. J. Theor. Phys.* **21**, 905 (1982).
- [12] J. M. Horowitz and H. Sandberg, Second-law-like inequalities with information and their interpretations, *New J. Phys.* **16**, 125007 (2014).
- [13] S. Still, Thermodynamic cost and benefit of memory, *Phys. Rev. Lett.* **124**, 050601 (2020).
- [14] S. Still and D. Daimer, Partially observable Szilard engines, *New J. of Physics (in press)*; (2022).
- [15] J. Ghojel, *Fundamentals of Heat Transfer* (John Wiley & Sons and ASME Press, 2020).
- [16] G. Paneru, S. Dutta, and H. K. Pak, Colossal power extraction from active cyclic Brownian information engines, *J. Phys. Chem. Lett.* **13**, 6912 (2022).
- [17] P. Magaretti and H. Stark, Szilard engines and information-based work extraction for active systems, *arXiv:2203.13075* (2022).
- [18] T. K. Saha, J. N. E. Lucero, J. Ehrich, D. A. Sivak, and J. Bechhoefer, Maximizing power and velocity of an information engine, *Proc. Natl. Acad. Sci. U.S.A.* **118**, 10.1073/pnas.2023356118 (2021).
- [19] I. A. Martínez, E. Roldan, J. M. R. Parrondo, and D. Petrov, Effective heating to several thousand kelvins of an optically trapped sphere in a liquid, *Phys. Rev. E* **87**, 032159 (2012).
- [20] M. Chupeau, B. Besga, D. Guéry-Odelin, E. Trizac, A. Petrosyan, and S. Ciliberto, Thermal bath engineering for swift equilibration, *Phys. Rev. E* **98**, 010104(R) (2018).
- [21] A. Militaru, A. Lasanta, M. Frimmer, L. L. Bonilla, L. Novotny, and R. A. Rica, Kovacs memory effect with an optically levitated nanoparticle, *Phys. Rev. Lett.* **127**, 130603 (2021).
- [22] R. Goerlich, L. B. Pires, G. Manfredi, P.-A. Hervieux, and C. Genet, Harvesting information to control non-equilibrium states of active matter, *arxiv:2112.10842* (2021).
- [23] A. E. Cohen, *Trapping and Manipulating Single Molecules in Solution*, Ph.D. thesis, Stanford University (2006).
- [24] P. Hänggi and P. Jung, Colored Noise in Dynamical Systems, *Adv. Chem. Phys.* **89**, 239 (1995).
- [25] G. Szamel, Self-propelled particle in an external potential: Existence of an effective temperature, *Phys. Rev. E* **90**, 012111 (2014).
- [26] R. Goerlich, L. B. Pires, G. Manfredi, P.-A. Hervieux, and C. Genet, Harvesting information to control non-equilibrium states of active matter, *arXiv:2112.10842* (2021).
- [27] A. Ghosh and A. J. Spakowitz, Statistical behavior of nonequilibrium and living biological systems subjected to active and thermal fluctuations, *Phys. Rev. E* **105**, 014415 (2022).
- [28] T. K. Saha, J. N. E. Lucero, J. Ehrich, D. A. Sivak, and J. Bechhoefer, Bayesian information engine that optimally exploits noisy measurements, *arXiv:2204.07310* (2022).
- [29] T. Franosch, M. Grimm, M. Belushkin, F. M. Mor, G. Foffi, L. Forró, and S. Jeney, Resonances arising from hydrodynamic memory in Brownian motion, *Nature* **478**, 85 (2011).
- [30] J. N. E. Lucero, J. Ehrich, J. Bechhoefer, and D. A. Sivak, Maximal fluctuation exploitation in gaussian information engines, *Phys. Rev. E* **104**, 044122 (2021).
- [31] T. M. Cover and J. A. Thomas, *Elements of Information Theory*, 2nd ed. (Wiley-Interscience, Hoboken, NJ, 2006).

- [32] J. Ehrlich, S. Still, and D. A. Sivak, Energetic cost of feedback control, [arXiv:2206.10793](https://arxiv.org/abs/2206.10793) (2022).
- [33] M. Smoluchowski, Experimentell nachweisbare, der üblichen Thermodynamik widersprechende Molekularphänomene, *Phys. Z.* **13**, 1069 (1912).
- [34] R. P. Feynman, R. B. Leighton, and M. Sands, *The Feynman Lectures on Physics* (Addison-Wesley, 1963) pp. 46.1–46.9.
- [35] J. M. R. Parrondo and P. Español, Criticism of Feynman’s analysis of the ratchet as an engine, *Am. J. Phys.* **64**, 1125 (1996).
- [36] H. Nyquist, Thermal agitation of electric charge in conductors, *Phys. Rev.* **32**, 110 (1928).
- [37] G. Stavrakakis, Electrical parts of wind turbines, in *Comprehensive Renewable Energy*, edited by A. Sayigh (Elsevier, 2012).
- [38] R. Watkins, *The Origins Of Self-Winding Watches 1773–1779*, 2nd ed. (NewPrint, Huntington, Tasmania, 2016).
- [39] P. Eshuis, K. van der Weele, D. Lohse, and D. van der Meer, Experimental realization of a rotational ratchet in a granular gas, *Phys. Rev. Lett.* **104**, 248001 (2010).
- [40] S. Joubaud, D. Lohse, and D. van der Meer, Fluctuation Theorems for an Asymmetric Rotor in a Granular Gas, *Phys. Rev. Lett.* **108**, 210604 (2012).
- [41] A. Gnoli, A. Petri, F. Dalton, G. Pontuale, G. Gradenigo, A. Sarracino, and A. Puglisi, Brownian Ratchet in a Thermal Bath Driven by Coulomb Friction, *Phys. Rev. Lett.* **110**, 120601 (2013).
- [42] A. Gnoli, S. A., A. Puglisi, and A. Petri, Nonequilibrium fluctuations in a frictional granular motor: Experiments and kinetic theory, *Phys. Rev. E* **87**, 052209 (2013).
- [43] M. Lagoin, C. Crauste-Thibierge, and A. Naert, The granular Brownian ratchet: carrying out a historical thought experiment, [hal-03650213 preprint](https://arxiv.org/abs/2203.03650) (2022).
- [44] F. Rouyer and N. Menon, Velocity fluctuations in a homogeneous 2d granular gas in steady state, *Phys. Rev. Lett.* **85**, 3676 (2000).
- [45] K. Feitosa and N. Menon, Fluidized Granular Medium as an Instance of the Fluctuation Theorem, *Phys. Rev. Lett.* **92**, 164301 (2004).
- [46] J.-Y. Chastaing, J.-C. Géminard, and A. Naert, Two methods to measure granular gas temperature, *J. Stat. Mech.* **2017**, 073212 (2017).
- [47] N. Francois, H. Xia, H. Punzmann, and M. Shats, Nonequilibrium Thermodynamics of Turbulence-Driven Rotors, *Phys. Rev. Lett.* **124**, 254501 (2020).
- [48] S. Mathew and G. S. Philip, Wind turbines: Evolution, basic principles, and classifications, in *Comprehensive Renewable Energy*, edited by A. Sayigh (Elsevier, 2012).
- [49] S. Ramaswamy, The Mechanics and Statistics of Active Matter, *Annu. Rev. Condens. Matter Phys.* **1**, 323 (2010).
- [50] M. C. Marchetti, J. F. Joanny, S. Ramaswamy, T. B. Liverpool, J. Prost, M. Rao, and R. Aditi Simha, Hydrodynamics of soft active matter, *Rev. Mod. Phys.* **85**, 1143 (2013).
- [51] A. Sokolov, M. M. Apodaca, B. A. Gryzbowski, and I. S. Aranson, Swimming bacteria power microscopic gears, *Proc. Nat. Acad. Sci.* **107**, 969 (2010).
- [52] R. Di Leonardo, L. Angelani, D. Dell’Arciprete, G. Ruocco, V. Iebba, S. Schippa, M. P. Conte, F. Mecarini, F. De Angelis, and E. Di Fabrizio, Bacterial ratchet motors, *Proc. Nat. Acad. Sci.* **107**, 9541 (2010).
- [53] C. J. Olson Reichhardt and C. Reichhardt, Ratchet Effects in Active Matter Systems, *Annu. Rev. Condens. Matter Phys.* **8**, 51 (2017).
- [54] G. Vizsnyiczai, G. Fangipane, C. Maggi, F. Saglimbeni, S. Bianchi, and R. Di Leonardo, Light controlled 3D micromotors powered by bacteria, *Nat. Comm.* **8**, 15974 (2017).
- [55] P. Pietzonka, E. Fodor, C. Lohrmann, M. E. Cates, and U. Seifert, Autonomous Engines Driven by Active Matter: Energetics and Design Principles, *Phys. Rev. X* **9**, 041032 (2019).
- [56] E. Fodor and M. E. Cates, Active engines: Thermodynamics moves forward, *Europhys. Lett.* **134**, 10003 (2021).
- [57] T. Speck, Stochastic thermodynamics for active matter, *Europhys. Lett.* **114**, 30006 (2016).
- [58] E. Fodor, C. Nardini, M. E. Cates, J. Tailleur, P. Visco, and F. van Wieland, How Far from Equilibrium Is Active Matter?, *Phys. Rev. Lett.* **117**, 038103 (2016).
- [59] D. Mandal, K. Klymko, and M. R. DeWeese, Entropy Production and Fluctuation Theorems for Active Matter, *Phys. Rev. Lett.* **119**, 258001 (2017).
- [60] P. Pietzonka and U. Seifert, Entropy production of active particles and for particles in active baths, *J. Phys. A: Math. Theor.* **51**, 01LT01 (2018).
- [61] L. Dabelow, S. Bo, and R. Eichhorn, Irreversibility in active matter systems: Fluctuation theorem and mutual information, *Phys. Rev. X* **9**, 021009 (2019).
- [62] L. Caprini, U. M. B. Marconi, A. Puglisi, and A. Vulpiani, The entropy production of Ornstein–Uhlenbeck active particles: a path integral method for correlations, *J. Stat. Mech.* **2019**, 053203 (2019).
- [63] L. Dabelow and R. Eichhorn, Irreversibility in active matter: General framework for active Ornstein-Uhlenbeck particles, *Front. in Phys.* **8**, 582992 (2021).
- [64] J. Elgeti, R. Winkler, and G. Gompper, Physics of microswimmers - single particle motion and collective behavior: a review, *Rep. Prog. Phys.* **78**, 056601 (2015).
- [65] C. Bechinger, R. Di Leonardo, H. Löwen, C. Reichhardt, G. Volpe, and G. Volpe, Active particles in complex and crowded environments, *Rev. Mod. Phys.* **88**, 045006 (2016).
- [66] D. Mizuno, C. Tardin, C. F. Schmidt, and F. C. MacKintosh, Nonequilibrium Mechanics of Active Cytoskeletal Networks, *Science* **315**, 370 (2007).
- [67] F. Gallet, D. Arcizet, P. Bohec, and A. Richert, Power spectrum of out-of-equilibrium forces in living cells: amplitude and frequency dependence, *Soft Matter* **5**, 2947 (2009).
- [68] T. Ariga, K. Tateishi, M. Tomishige, and D. Mizuno, Noise-Induced Acceleration of Single Molecule Kinesin-1, *Phys. Rev. Lett.* **127**, 178101 (2021).
- [69] A. K. Tripathi, T. Das, G. Paneru, G. K. Pak, and T. Thusty, Acceleration of enzymatic catalysis by active hydrodynamic fluctuations, *Comm. Phys.* **8**, 101 (2022).
- [70] S. P. Beeby, M. J. Tudor, and N. M. White, Energy harvesting vibration sources for microsystems applications, *Meas. Sci. Technol.* **17**, R175 (2006).
- [71] S. Priya, Advances in energy harvesting using low profile piezoelectric transducers, *J. Electroceram.* **19**, 165 (2007).
- [72] K. A. Cook-Chennault, N. Thambi, and A. M. Sastry, Powering MEMS portable devices—a review of non-regenerative and regenerative power supply systems with special emphasis on piezoelectric energy harvesting systems, *Smart Mater. Struct.* **17**, 043001 (2008).

- [73] P. D. Mitcheson, E. M. Yeatman, G. K. Rao, A. S. Holmes, and T. C. Green, Energy Harvesting From Human and Machine Motion for Wireless Electronic Devices, *Proceedings of the IEEE* **96**, 1457 (2008).
- [74] L. Gammaitoni, H. Vocca, I. Neri, F. Travasso, and F. Orfei, Vibration Energy Harvesting: Linear and Nonlinear Oscillator Approaches, in *Sustainable Energy Harvesting Technologies - Past, Present and Future*, edited by T. Y. Kheng (IntechOpen, 2011) Chap. 7.
- [75] F. Liu, Y. Zhang, O. Dahlsten, and F. Wang, Intelligently chosen interventions have potential to outperform the diode bridge in power conditioning, *Nature Sci. Rep.* **9**, 8994 (2019).
- [76] B. J. Lopez, N. J. Kuwada, E. M. Craig, B. R. Long, and H. Linke, Realization of a feedback controlled flashing ratchet, *Phys. Rev. Lett.* **101**, 220601 (2008).
- [77] A. Kumar and J. Bechhoefer, Nanoscale virtual potentials using optical tweezers, *Appl. Phys. Lett.* **113**, 183702 (2018).
- [78] D. H. Wolpert, A. Kolchinsky, and J. A. Owen, A space-time tradeoff for implementing a function with master equation dynamics, *Nat. Commun.* **10**, 1727 (2019).
- [79] W. S. Bialek, *Biophysics: Searching for Principles* (Princeton University Press, Princeton, NJ, 2012).
- [80] J. Ehrich, https://github.com/JannikEhrich/Information_engine_in_a_nonequilibrium_bath (2022).